Instability of a leaky dielectric coaxial jet in both axial and radial electric fields

Fang Li, Xie-Yuan Yin, and Xie-Zhen Yin*
Department of Modern Mechanics, University of Science and Technology of China, Hefei, Anhui 230027, People's Republic of China
(Received 31 March 2008; revised manuscript received 16 July 2008; published 4 September 2008)

The temporal linear instability of a coaxial jet with two immiscible Newtonian liquids in both the axial and radial electric fields is studied. The outer liquid is supposed to be a leaky dielectric and the inner liquid a perfect dielectric. The eigenvalue problem for both axisymmetric instability and helical instability is formulated and solved using the spectral method. Different from axisymmetric instability, for helical instability there is only one unstable mode, i.e., the helical mode, located in the long wave region. The axial electric field is found to have a strong stabilization effect on both the axisymmetric and helical modes, and the radial electric field has a great destabilization effect on them. The competition between the axisymmetric and helical instability under the action of the axial and radial electric fields is calculated. The boundary curve separating the stabilization and destabilization regions of the parasinuous mode, the neutral stability curve of the helical mode, and the boundary curve between the dominant regions of the axisymmetric and helical instability are plotted on the Q_0-E_u plane and Π-E_u plane, respectively (Q_0 is the dimensionless surface charge density; E_u is the electrical Euler number representing the characteristic tangential electrostatic force; and $\Pi=Q_0^2E_u$ is the dimensionless parameter representing the characteristic normal electrostatic force). In general, when surface charge density is small, the helical mode is stable, and the parasinuous mode is dominant; however, when surface charge density is sufficiently large, the helical mode is destabilized and becomes dominant in jet instability. Liquid viscosity influences the predominance of the helical mode significantly. Although liquid viscosity decreases the growth rates of both the axisymmetric and helical modes, it suppresses the axisymmetric instability much more than the helical instability, and therefore favors the realization of the helical instability in experiments.

DOI: 10.1103/PhysRevE.78.036302 PACS number(s): 47.20.−k, 47.65.−d, 47.15.Fe

I. INTRODUCTION

The research on instability of an electrified liquid jet is of both theoretical and practical interest. The early research is mainly focused on the linear instability behavior of jets in an electric field. The basic velocity profile of jets is assumed to be uniform and the liquid is considered to be perfectly conducting. In such a case free charge is located on the jet surface with zero electrical shear force. The earliest research ascends to Rayleigh's work [1]. He found that electric field may stabilize disturbances of long wavelength in the case of axisymmetric instability, but destabilize disturbances of short wavelength. Zeleny [2] later examined the instability of an electrified liquid surface. Taylor [3–6] studied the instability of an inviscid jet in electric field both theoretically and experimentally. He also calculated the growth rates of the varicose mode and kink mode under the approximation of small perturbation. Melcher [7] studied the effect of free charge on the instability of a conducting inviscid liquid jet. He pointed out that in a moderate electric field the axisymmetric mode is the least stable. Saville [8,9] established a theoretical model of a viscous liquid jet in a tangential electric field, taking into account the effect of the electrical relaxation time. He found that under the action of the electric field and liquid viscosity, the least stable mode is the varicose mode in the long wave region. Moreover, the tangential electric field suppresses the growth of disturbances, and enlarges the intact length of jets. Huebner and Chu [10] analyzed the instability of electrified jets in the limit of zero viscosity. They found that the least stable wavelength decreases as charge increases. When charge density is sufficiently large, transition of the least stable mode occurs, from axisymmetric to nonaxisymmetric.

In the past decade, the instability of electrified liquid jets has been excessively studied. Artana *et al.* [11] and Baudry *et al.* [12] analyzed the instability of an electrified inviscid liquid jet at high velocity. They discussed the effects of the electric field, jet velocity, liquid properties, and ambient air on the temporal growth rate of unstable waves. Son and Ohba [13] compared theoretically and experimentally the axisymmetric and nonaxisymmetric instability of an inviscid liquid jet in an electric field of needle-plane configuration. González *et al.* [14] and González *et al.* [15] investigated the effect of a radial ac electric field on the instability of a conducting viscous liquid jet and found that the parametric resonance between the natural dc frequency and imposed ac frequency may lead to the destabilization of the jet in the stable region, which is considered to be a possible way to produce droplets of small size. Using the Taylor-Melcher leaky dielectric model [16,17], López-Herrera *et al.* [18] analyzed the axisymmetric instability of a viscous liquid jet of low conductivity in a radial electric field. They found that the relative electrical relaxation time and relative electrical permittivity have a significant effect on the growth rate and least stable wavelength. Turnbull [19,20] studied the axisymmetric instability of a viscous liquid jet under the action of both axial and radial electric fields, where the liquid was assumed to be either perfectly dielectric or leaky dielectric. Mestel [21,22] analyzed the instability of a charged liquid jet in an axial electric field. He derived the dispersion relation under the low viscosity and high viscosity approximations, respec-

*xzyin@ustc.edu.cn

tively. Several limit cases were discussed there.

As to nonlinear instability analysis, to date most research has been focused on the weakly nonlinear instability behaviors of electrified liquid jets. Setiawan and Heister [23] extended the work of Huebner and Chu [10] to the nonlinear domain. They investigated the axisymmetric breakup of an inviscid conducting liquid jet in a high electric field. Elhefnawy *et al.* [24] performed the nonlinear instability analysis of a conducting jet in an axial electric field, and Elhefnawy *et al.* [25] analyzed the nonlinear instability of a conducting cylinder in a radial electric field. Elcoot [26,27] extended the work of Elhefnawy *et al.* [24,25] to the leaky dielectric case. In addition, Elcoot [28] extended the nonlinear instability analysis to the viscous case, considering the effect of liquid viscosity on the normal force balance at the interface.

As observed in experiments [13,29], electrified jets may undergo different modes when destabilized, either breaking into droplets or behaving like a whip without breaking. More attractively, when a coaxial jet with one liquid coated with the other is subjected to electric field, it produces microcapsules or ultrathin composite fibers [30–33]. The former is known as coaxial electrospraying, and the latter as coaxial electrospinning. In the coaxial electrospraying process, axisymmetric disturbances dominate the instability of the jet and the jet breaks up into compound droplets ultimately [30,31]. Differently, in the coaxial electrospinning process, the helical instability becomes dominant, and the coaxial jet bends in the three-dimensional space without breakup [32,33]. These different behaviors of jets are closely associated with the instability mechanism of coaxial jets in an electric field, which has been rarely studied.

The authors performed the instability analysis of an electrified coaxial liquid jet. The effects of the radial and axial electric fields on the unstable modes of an inviscid coaxial jet were studied [34–36]. In a recent paper [37], the authors investigated the axisymmetric instability of a viscous coaxial jet in a radial electric field, where the outer driving liquid was assumed to be a leaky dielectric. In order to obtain analytical dispersion relations, the basic velocity profile was simplified there. In the present paper we establish a more complex model, extending the work of [37]. An exact nonuniform basic velocity profile derived from the steady Navier-Stokes equations is used, and therefore an analytical dispersion relation is beyond reach. The eigenvalues in the temporal linear analysis are calculated using the spectral method. Besides the axial electric field, surface charge is imposed on the outer air-liquid interface to provide a radial electric field. Besides the axisymmetric instability (the azimuthal wave number $n=0$), the helical instability ($n=1$) is studied. The competition between the axisymmetric and helical instability is carried out. The effect of liquid viscosity on the predominance of the helical mode is also studied. It is evident that the model used in the present paper is more rational and complicated than that in [37].

The paper is organized as follows. In Sec. II, the theoretical model is described and the eigenvalue problem is formulated in detail. In Sec. III, the unstable modes are calculated numerically. The effects of the axial and radial electric fields on the jet instability and the comparisons between the axisymmetric and helical modes are discussed. In Sec. IV, main conclusions are drawn.

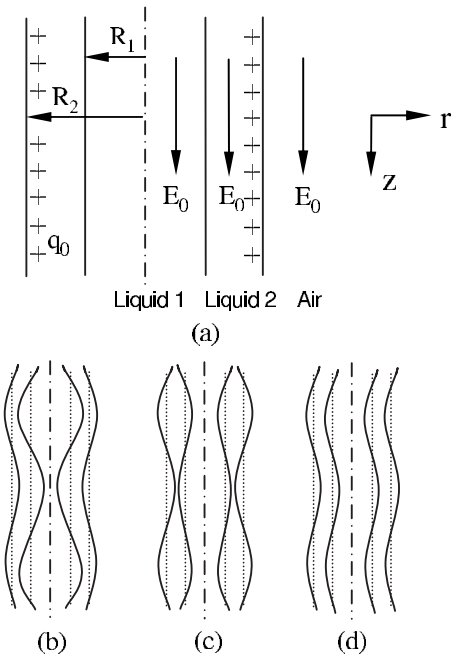

FIG. 1. (a) Schematic of the theoretical model. The radii of liquid 1 and liquid 2 are R_1 and R_2, respectively. The system is subjected to an axial electric field of magnitude E_0. Besides, there is free charge of density q_0 on the interface between liquid 2 and air. (b) The parasinuous mode, (c) the paravaricose mode, and (d) the helical mode.

II. THEORETICAL MODEL

We propose a theoretical model similar to that developed in [21,22]. The difference lies in that a two-liquid coaxial jet case is considered instead of a single-liquid jet in the present model. As shown in Fig. 1(a), an infinitely long coaxial cylindrical jet consists of two immiscible viscous Newtonian liquids, surrounded by air. The inner and outer liquids have constant radii R_1 and R_2, respectively. It is assumed that the hydrodynamic effects of the air and gravity are negligible. The outer liquid is supposed to be a leaky dielectric with finite electrical conductivity; the inner liquid and air are perfectly dielectrics. The liquids and air are subjected to a uniform axial electric field E_0. Besides the axial electric field, free charge of density q_0 is imposed on the outer air-liquid interface, providing a radial electric field of magnitude $q_0 R_2/\varepsilon_3 r$ in the air, where ε_3 is the permittivity of the air and r is the axial coordinate in the cylindrical coordinate system (r,θ,z). Therefore in the unperturbed state the basic electric field in the dimensionless form is

$$\mathbf{E}_1 = (0,0,1),$$

$$\mathbf{E}_2 = (0,0,1),$$

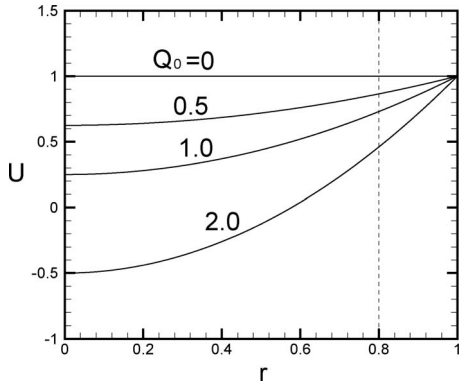

FIG. 2. Effect of the dimensionless surface charge density Q_0 on the basic velocity profile $U_z(r)$. $E_u=0.15$, $R_e=10$, $a=0.8$, and $\mu_r=1$.

$$\mathbf{E}_3 = \left(\frac{Q_0}{r}, 0, 1\right),$$

where the subscripts 1, 2, and 3 denote the inner liquid, the outer liquid, and the air, respectively. Here R_2, E_0, and $\varepsilon_3 E_0$ are chosen as the characteristic length, electric field intensity, and free charge density, respectively. The dimensionless surface charge density $Q_0=q_0/\varepsilon_3 E_0$.

Suppose the basic flow is steady and axisymmetric. The basic velocity has only the component in the axial direction, i.e., $U_z(r)$. Under the influence of the axial electric field and surface free charge, the basic velocity profile satisfying the steady momentum equations and boundary conditions are [21,37]

$$U_{1z} = 1 + \frac{Q_0 E_u R_e}{2}(a^2 - 1) + \frac{Q_0 E_u R_e}{2\mu_r}(r^2 - a^2),$$

$$U_{2z} = 1 + \frac{Q_0 E_u R_e}{2}(r^2 - 1),$$

where the dynamic viscosity, velocity, and pressure are scaled by μ_2, $U_{2\text{out}}$ [the velocity at the outer air-liquid interface, $U_{2\text{out}}=U_{2z}(R_2)$], and $\rho_2 U_{2\text{out}}^2$, respectively. The radius ratio $a=R_1/R_2$, the viscosity ratio $\mu_r=\mu_1/\mu_2$, the Reynolds number $R_e=\rho_2 U_{2\text{out}} R_2/\mu_2$, and the electrical Euler number $E_u=\varepsilon_3 E_0^2/\rho_2 U_{2\text{out}}^2$.

Figure 2 illustrates the effect of the dimensionless surface charge density Q_0 on the basic velocity profile $U_z(r)$. As shown in the figure, the inner and outer liquids of the coaxial jet have the same velocity when surface charge vanishes ($Q_0=0$). As Q_0 increases, the basic velocity profile becomes nonuniform. This is because surface charge and axial electric field produce electrical shear force at the outer air-liquid interface, which, together with liquid viscosity, induces the nonuniformity of velocity in the liquids.

The dimensionless linearized equations governing the flow are

$$\nabla \cdot \mathbf{u}_m = 0, \tag{1}$$

$$\frac{\partial \mathbf{u}_m}{\partial t} + \mathbf{u}_m \cdot \nabla \mathbf{U}_m + \mathbf{U}_m \cdot \nabla \mathbf{u}_m = -\left(\frac{1}{S}\delta_{m1} + \delta_{m2}\right)\nabla p_m + \left(\frac{\mu_r}{S}\delta_{m1} + \delta_{m2}\right)\frac{1}{R_e}\nabla^2 \mathbf{u}_m, \tag{2}$$

for $m=1,2$, where $\mathbf{u}$ and p are the perturbations of the velocity and pressure, respectively, the density ratio $S=\rho_1/\rho_2$, and δ is the Kronecker function.

At the symmetric axis $r=0$, the axisymmetric instability case $n=0$ and the helical instability case $n=1$ have different boundary conditions, i.e.,

$$u_{1r} = \frac{\partial u_{1z}}{\partial r} = \frac{\partial p_1}{\partial r} = 0 \quad \text{for } n = 0, \tag{3}$$

$$u_{1z} = p_1 = 0, \quad u_{1r} + \frac{\partial u_{1\theta}}{\partial \theta} = 0, \quad 2\frac{\partial u_{1r}}{\partial r} + \frac{\partial^2 u_{1\theta}}{\partial r \partial \theta} = 0 \quad \text{for } n = 1, \tag{4}$$

where u_r, u_θ, and u_z are the velocity components in the r, θ, and z directions, respectively. At the inner liquid-liquid interface $r=a+\eta_1$ and outer air-liquid interface $r=1+\eta_2$, the kinematic boundary conditions and the continuity of the velocity should be satisfied, i.e.,

$$u_{mr} = \left(\frac{\partial}{\partial t} + U_{mz}\frac{\partial}{\partial z}\right)\eta_1, \quad m = 1,2, \tag{5}$$

$$u_{1z} + \frac{dU_{1z}}{dr}\eta_1 = u_{2z} + \frac{dU_{2z}}{dr}\eta_1, \tag{6}$$

$$u_{2r} = \left(\frac{\partial}{\partial t} + U_{2z}\frac{\partial}{\partial z}\right)\eta_2, \tag{7}$$

$$u_{1\theta} = u_{2\theta}, \tag{8}$$

where η_j, $j=1,2$, is the displacement of the interface from its equilibrium position R_j. The subscripts 1 and 2 denote the inner liquid-liquid and outer air-liquid interfaces, respectively. The dynamic boundary conditions are

$$\frac{\partial u_{2r}}{\partial z} + \frac{\partial u_{2z}}{\partial r} + \frac{d^2 U_{2z}}{dr^2}\eta_1 - \mu_r\left(\frac{\partial u_{1r}}{\partial z} + \frac{\partial u_{1z}}{\partial r} + \frac{d^2 U_{1z}}{dr^2}\eta_1\right) = 0, \tag{9}$$

$$\frac{\partial u_{2r}}{r\partial \theta} + \frac{\partial u_{2\theta}}{\partial r} - \frac{u_{2\theta}}{r} - \mu_r\left(\frac{\partial u_{1r}}{r\partial \theta} + \frac{\partial u_{1\theta}}{\partial r} - \frac{u_{1\theta}}{r}\right) = 0, \tag{10}$$

$$p_1 - \frac{2\mu_r}{R_e}\frac{\partial u_{1r}}{\partial r} - p_2 + \frac{2}{R_e}\frac{\partial u_{2r}}{\partial r} + \frac{E_u}{2}(\varepsilon_{r1}E_{1z}^2 - \varepsilon_{r2}E_{2z}^2) = \frac{\Gamma}{W_e}\nabla \cdot \mathbf{n}_1, \tag{11}$$

$$\frac{1}{R_e}\left(\frac{\partial u_{2r}}{\partial z}+\frac{\partial u_{2z}}{\partial r}+\frac{d^2U_{2z}}{dr^2}\eta_2\right)+\varepsilon_{r2}E_uE_{2r}-E_uE_{3r}-Q_0E_uE_{3z}-n_{2z}E_u(1-Q_0^2-\varepsilon_{r2})=0, \tag{12}$$

$$\frac{1}{R_e}\left(\frac{\partial u_{2r}}{r\partial\theta}+\frac{\partial u_{2\theta}}{\partial r}-\frac{u_{2\theta}}{r}\right)-Q_0E_uE_{3\theta}+Q_0^2E_un_{2\theta}=0, \tag{13}$$

$$p_2-\frac{2}{R_e}\frac{\partial u_{2r}}{\partial r}+\frac{1}{2}E_u(E_{3r}^2-E_{3z}^2+\varepsilon_{r2}E_{2z}^2)=\frac{1}{W_e}\nabla\cdot\mathbf{n}_2, \tag{14}$$

where $\mathbf{n}_j$, $j=1,2$ is the normal unit vector on the interface, E is the electric field component, the Weber number $W_e=\rho_2U_{2\text{out}}^2R_2/\gamma_2$, and the surface tension ratio $\Gamma=\gamma_1/\gamma_2$.

As to electric field, the electrical potential perturbation ψ_m satisfies the Laplace equation:

$$\nabla^2\psi_m=0,\quad m=1,2,3. \tag{15}$$

The electric field intensity $\mathbf{E}_m=-\nabla\psi_m$. At the symmetric axis $r=0$ and infinity $r\to\infty$, the electric field should be finite, i.e.,

$$\mathbf{E}_1<\infty,\quad \mathbf{E}_3<\infty. \tag{16}$$

At the inner and outer interfaces, the continuity of the tangential electric field and the Gauss law should be satisfied, i.e.,

$$\mathbf{n}_j\times[\mathbf{E}]=0,\quad j=1,2, \tag{17}$$

$$\mathbf{n}_1\times(\varepsilon_{r2}\mathbf{E}_2-\varepsilon_{r1}\mathbf{E}_1)=0, \tag{18}$$

$$\mathbf{n}_2\cdot(\mathbf{E}_3-\varepsilon_{r2}\mathbf{E}_2)=q_s, \tag{19}$$

where the symbol $[\cdot]$ denotes the jump of a quantity across the interface, the electrical permittivity ratios $\varepsilon_{r1}=\varepsilon_1/\varepsilon_3$, $\varepsilon_{r2}=\varepsilon_2/\varepsilon_3$, and q_s is the perturbation of the surface charge density at the outer interface, satisfying the surface charge conservation equation [16,17]

$$\frac{\partial q_s}{\partial t}+U_{2z}\frac{\partial q_s}{\partial z}-Q_0\mathbf{n}_2\cdot(\mathbf{n}_2\cdot\nabla)\mathbf{u}_2-\tau\varepsilon_{r2}\mathbf{E}_2\cdot\mathbf{n}_2=0, \tag{20}$$

with the relative electrical relaxation time $\tau=R_2\sigma_2/U_{2\text{out}}\varepsilon_2$.

In the temporal instability analysis, any infinitesimal disturbance can be decomposed into the form of a Fourier exponential, i.e.,

$$\phi(r,\theta,z,t)=\hat{\phi}(r)e^{\omega t+i(kz+n\theta)},$$

where ω is the complex eigenfrequency, the real and imaginary parts of which are the temporal growth rate and frequency, respectively, k is the axial wave number (real), n is the azimuthal wave number (integer), and i is the imaginary unit. Note that the electromechanical coupling occurs only at the outer interface. We solve the electric field individually and only keep the surface charge density $\hat{q}_s$ as the unknown quantity. Some details are given in Appendix A. Substituting the decomposition into Eqs. (1)–(20), we obtain the following ordinary differential equations and boundary conditions:

$$\frac{d\hat{u}_{mr}}{dr}+\frac{\hat{u}_{mr}}{r}+\frac{i\delta_{n1}}{r}\hat{u}_{1\theta}+ik\hat{u}_{mz}=0, \tag{21}$$

$$\omega\hat{u}_{mr}=-\left(\frac{1}{S}\delta_{m1}+\delta_{m2}\right)\frac{d\hat{p}_m}{dr}+\frac{1}{R_e}\left(\frac{\mu_r}{S}\delta_{m1}+\delta_{m2}\right)\left\{\frac{d^2}{dr^2}+\frac{1}{r}\frac{d}{dr}-\left[k^2+\frac{1+\delta_{n1}}{r^2}+ikR_eU_{mz}\left(\frac{S}{\mu_r}\delta_{m1}+\delta_{m2}\right)\right]\right\}\hat{u}_{mr}-\frac{2i\delta_{n1}}{r^2R_e}\left(\frac{\mu_r}{S}\delta_{m1}+\delta_{m2}\right)\hat{u}_{m\theta}, \tag{22}$$

$$\omega\hat{u}_{mz}=-\frac{dU_{mz}}{dr}\hat{u}_{mr}-ik\left(\frac{1}{S}\delta_{m1}+\delta_{m2}\right)\hat{p}_m+\frac{1}{R_e}\left(\frac{\mu_r}{S}\delta_{m1}+\delta_{m2}\right)\times\left\{\frac{d^2}{dr^2}+\frac{1}{r}\frac{d}{dr}-\left[k^2+\frac{\delta_{n1}}{r^2}+ikR_eU_{mz}\left(\frac{S}{\mu_r}\delta_{m1}+\delta_{m2}\right)\right]\right\}\hat{u}_{mz}, \tag{23}$$

$$\omega\hat{u}_{m\theta}=-\frac{i}{r}\left(\frac{1}{S}\delta_{m1}+\delta_{m2}\right)\hat{p}_m+\frac{1}{R_e}\left(\frac{\mu_r}{S}\delta_{m1}+\delta_{m2}\right)\left\{\frac{d^2}{dr^2}+\frac{1}{r}\frac{d}{dr}-\left[k^2+\frac{2}{r^2}+ikR_eU_{mz}\left(\frac{S}{\mu_r}\delta_{m1}+\delta_{m2}\right)\right]\right\}\hat{u}_{m\theta}+\frac{2i}{r^2R_e}\left(\frac{\mu_r}{S}\delta_{m1}+\delta_{m2}\right)\hat{u}_{mr}; \tag{24}$$

at the symmetric axis,

$$\hat{u}_{1r}=\frac{d\hat{u}_{1z}}{dr}=\frac{d\hat{p}_1}{dr}=0\quad\text{for } n=0, \tag{25}$$

$$\hat{u}_{1z}=\hat{p}_1=0,\quad \hat{u}_{1r}+i\hat{u}_{1\theta}=0,\quad 2\frac{d\hat{u}_{1r}}{dr}+i\frac{d\hat{u}_{1\theta}}{dr}=0\quad\text{for } n=1; \tag{26}$$

at the inner interface $r=a+\eta_1$,

$$\omega\hat{\eta}_1=\hat{u}_{1r}-ikU_{1z}\hat{\eta}_1,\quad \hat{u}_{1r}=\hat{u}_{2r},\quad \hat{u}_{1\theta}=\hat{u}_{2\theta}, \tag{27}$$

$$\hat{u}_{1z}-\hat{u}_{2z}+\left(\frac{dU_{1z}}{dr}-\frac{dU_{2z}}{dr}\right)\hat{\eta}_1=0, \tag{28}$$

$$ik\hat{u}_{2r}+\frac{d\hat{u}_{2z}}{dr}-\mu_r\left(ik\hat{u}_{1r}+\frac{d\hat{u}_{1z}}{dr}\right)+\left(\frac{d^2U_{2z}}{dr^2}-\mu_r\frac{d^2U_{1z}}{dr^2}\right)\hat{\eta}_1=0, \tag{29}$$

$$\frac{i}{a}\hat{u}_{2r}+\frac{d\hat{u}_{2\theta}}{dr}-\frac{\hat{u}_{2\theta}}{a}-\mu_r\left(\frac{i}{a}\hat{u}_{1r}+\frac{d\hat{u}_{1\theta}}{dr}-\frac{\hat{u}_{1\theta}}{a}\right)=0, \tag{30}$$

$$\hat{p}_1 - \frac{2\mu_r}{R_e}\frac{d\hat{u}_{1r}}{dr} - \hat{p}_2 + \frac{2}{R_e}\frac{d\hat{u}_{2r}}{dr} + \hat{q}_s \cdot ik^2 E_u(\varepsilon_{r2} - \varepsilon_{r1}) \times (D_3\Delta_1 + D_6\Delta_0) + \hat{\eta}_1\left(ik^2 E_u(\varepsilon_{r2} - \varepsilon_{r1})(D_4\Delta_1 + D_7\Delta_0) + \frac{\Gamma}{W_e a^2}[\delta_{n0} - (ak)^2]\right) + \hat{\eta}_2 \cdot ik^2 E_u(\varepsilon_{r2} - \varepsilon_{r1})(D_5\Delta_1 + D_8\Delta_0) = 0; \quad (31)$$

at the outer interface $r=1+\eta_2$,

$$\omega\hat{\eta}_2 = \hat{u}_{2r} - ikU_{2z}\hat{\eta}_2, \quad (32)$$

$$ik\hat{u}_{2r} + \frac{d\hat{u}_{2z}}{dr} + \hat{q}_s \cdot R_e E_u(ikQ_0 D_3 - 1) + \hat{\eta}_1 \cdot ikQ_0 R_e E_u D_4 + \hat{\eta}_2\left(\frac{d^2 U_{2z}}{dr^2} + ikQ_0 R_e E_u D_5\right) = 0, \quad (33)$$

$$i\hat{u}_{2r} + \frac{d\hat{u}_{2\theta}}{dr} - \hat{u}_{2\theta} + iQ_0 R_e E_u(\hat{q}_s D_3 + \hat{\eta}_1 D_4 + \hat{\eta}_2 D_5) = 0, \quad (34)$$

$$\hat{p}_2 - \frac{2}{R_e}\frac{d\hat{u}_{2r}}{dr} + \hat{q}_s \cdot E_u[Q_0(1 - k\varepsilon_{r2}D_6) + ikD_3(1 - \varepsilon_{r2})] + \hat{\eta}_1 \cdot E_u[-k\varepsilon_{r2}Q_0 D_7 + ikD_4(1 - \varepsilon_{r2})] + \hat{\eta}_2\left(E_u[ikQ_0(2 - \varepsilon_{r2}) - k\varepsilon_{r2}Q_0 D_8 + ikD_5(1 - \varepsilon_{r2})] + \frac{\delta_{n0} - k^2}{W_e}\right) = 0, \quad (35)$$

$$\hat{q}_s(\omega + ik + k\tau\varepsilon_{r2}D_6) - Q_0\frac{d\hat{u}_{2r}}{dr} + \hat{\eta}_1 \cdot k\tau\varepsilon_{r2}D_7 + \hat{\eta}_2\left(ikQ_0\frac{dU_{2z}}{dr} + k\tau\varepsilon_{r2}(D_8 + i)\right) = 0, \quad (36)$$

where the expressions of the symbols Δ_1, Δ_2, and D_1–D_8 are given in Appendix B. Equations (21)–(36) provide all the equations the numerical procedure needs. The eigenfunctions include $\hat{u}_{1r}$, $\hat{u}_{1z}$, $\hat{p}_1$, $\hat{u}_{2r}$, $\hat{u}_{2z}$, $\hat{p}_2$, $\hat{\eta}_1$, $\hat{\eta}_2$, and $\hat{q}_s$ for both the axisymmetric and helical cases, and additional $\hat{u}_{1\theta}$, $\hat{u}_{2\theta}$ for the helical case.

III. NUMERICAL RESULTS

Because of the consideration of viscosity and nonuniform basic velocity profile, it is impossible to obtain an analytical dispersion relation as implemented in [21,22,34–37]. So we use the Chebyshev spectral collocation method to solve the eigenvalue problem numerically. For the inner liquid, the number of the collocation points is commonly 10–15; for the outer liquid, the number is 5–10. A MATLAB code is developed to solve the corresponding generalized eigenvalue problem. The code has been verified by the result in [37] before calculation.

As is well-known, for the axisymmetric instability $n=0$ there are two unstable modes in the Rayleigh regime [34–37]. Different from a planar liquid jet, for a cylindrical coaxial jet having two interfaces the phase difference of the inner and outer interface disturbances is not exactly 0° (the sinuous mode) or 180° (the varicose mode). Therefore the one with a phase difference close to 0° is called parasinuous mode [as shown in Fig. 1(b)], and the other with a phase difference close to 180° is called paravaricose mode [Fig. 1(c)] [38,39]. For the helical instability $n=1$, the calculation result indicates that there is only one unstable mode. As shown in Fig. 1(d), the inner and outer interfaces are perturbed almost in the same phase, and the central line is modulated with cross section keeping constant. We call it the helical mode. In the numerical part we investigate the effects of the axial and radial electric fields on these unstable modes.

For convenience of calculation and comparison, we take water and sunflower oil as the outer and inner liquids [2], respectively. Suppose a reference state. The reference dimensionless parameters are $S=0.84$, $a=0.8$, $\mu_r=43$, $R_e=10$, $W_e=10$, $\Gamma=0.23$, $\varepsilon_{r1}=3.4$, $\varepsilon_{r2}=80$, and $\tau=1$. In the calculation the dimensionless parameters are fixed to the reference values except when clarified otherwise.

A. Effect of the axial and radial electric fields

The consideration of both the axial and radial electric fields makes the problem complex. The electrical Euler number E_u represents the effect of the axial electric field. As E_u increases, the axial electric field becomes stronger. On the other hand, E_u together with the dimensionless surface charge density Q_0 represents the effect of the surface charge (i.e., the radial electric field). As E_u and Q_0 increase, the radial electric field is amplified. For convenience, we investigate their effects through changing the electrical Euler number at low and high surface charge densities, respectively.

When the surface charge density is sufficiently low, the helical mode has negative growth rate and hence is stable. However, the axisymmetric modes may possess positive growth rate, indicating that the axisymmetric modes are unstable. Figures 3(a) and 3(b) illustrate the growth rates of the paravaricose mode and parasinuous mode, respectively, where the surface charge density is kept null. In the absence of surface charge, the radial electric field vanishes. Consequently the coaxial jet is purely under the influence of an axial electric field. In the figure it is clear that the axial electric field has a stabilizing effect on both the paravaricose mode and parasinuous mode. Particularly, the paravaricose mode is remarkably suppressed and becomes stable even when the electric field is small. The phenomenon is accordant with the instability of an inviscid coaxial jet in the axial electric field [36]. In such a case, the parasinuous mode is the most unstable, and therefore dominates in jet instability. This result agrees well with coaxial electrospraying experiments [31].

When the surface charge density is sufficiently high, the radial electric field has a more profound effect on jet instability than the axial electric field. In such a case, the helical

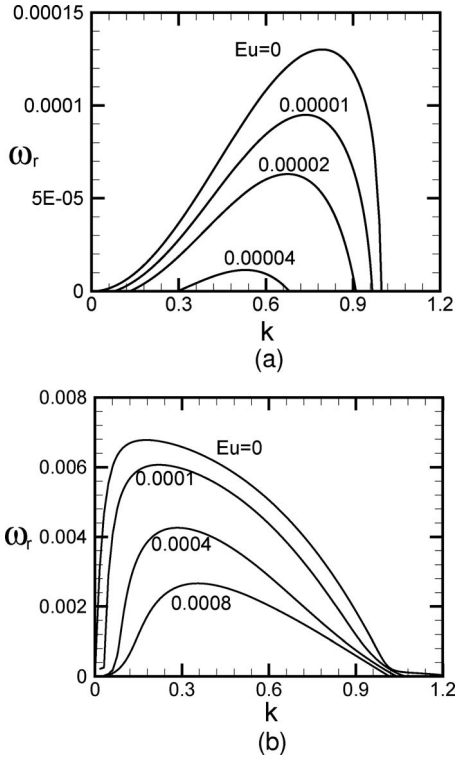

FIG. 3. Influence of the electrical Euler number E_u on the growth rate ω_r of (a) the paravaricose mode and (b) the parasinuous mode at zero surface charge density. $Q_0=0$.

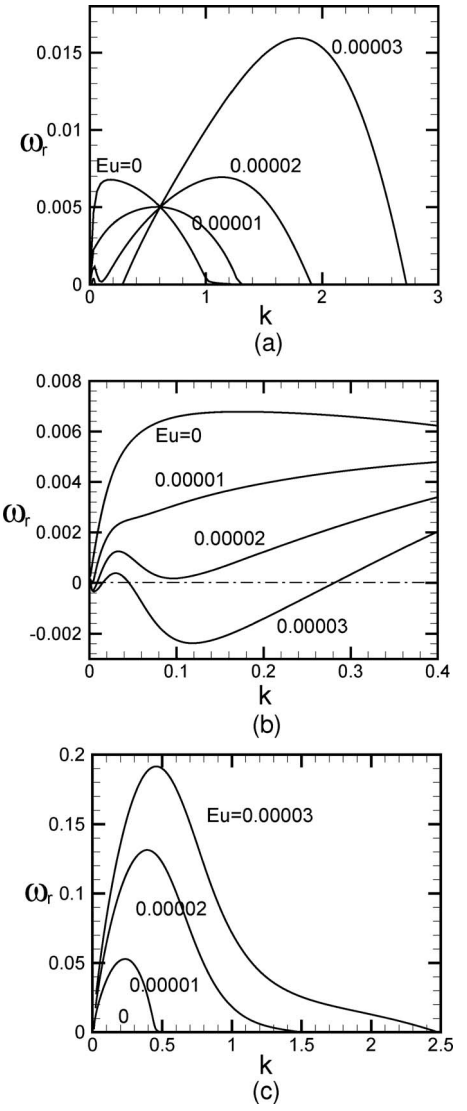

FIG. 4. Influence of the electrical Euler number E_u on the growth rate ω_r of (a) the parasinuous mode and (c) the helical mode at high surface charge density. $Q_0=100$. (b) The growth rate of the parasinuous mode in the long wavelength region [corresponding to (a)].

mode becomes unstable and probably dominates jet instability instead of the axisymmetric modes. Figures 4(a) and 4(c) illustrate the growth rates of the parasinuous mode and helical mode, respectively, as electric field varies. The dimensionless surface charge density is kept at 100. As shown in Fig. 4(a), the radial electric field has a twofold effect on the growth rate of the parasinuous mode. When the wave number exceeds a critical value (the critical wave number $k_c \approx 0.6$, which is not affected by electric field) the parasinuous mode is destabilized by the radial electric field. However, in the long wave region where the wave number is smaller than the critical value the parasinuous mode is stabilized. For more details see Fig. 4(b). The twofold effect of radial electric field on the axisymmetric instability was also found in the study of an inviscid coaxial jet [35] and a viscous coaxial jet in the absence of an axial electric field [37]. It turns out to be the inherent characteristic of the radial electric field. On the other hand, the radial electric field has a significant destabilization effect on the helical mode, as shown in Fig. 4(c). Comparing Fig. 4(c) with Fig. 4(a), it is clear that the growth rate of the helical mode is much higher than that of the parasinuous mode, indicating that the helical mode is the most unstable. The result predicts that in a sufficiently strong radial electric field the helical mode may be predominant in the process of jet breakup. That is, strong radial electric field favors the realization of coaxial electrospinning in experiments.

To illuminate the effect of the axial and radial electric fields further, we investigate the characteristics of the parasinuous and helical modes, respectively, on the parameter planes. For the parasinuous mode, we compare its maximum growth rates at different values of Q_0 and E_u with that at zero electric field and obtain the boundary curve separating the stabilization and destabilization regions on the Q_0-E_u plane, as plotted in Fig. 5(a). In the region marked with "destabilize," the combined axial and radial electric field has a destabilization effect on the parasinuous mode. However, in the region marked with "stabilize," the electric field stabilizes the mode. It is clear that when the surface charge density is sufficiently large the radial electric field is much more profound. Therefore the mode is destabilized even when E_u is considerably small. On the other hand, if the surface charge is sufficiently small, the axial electric field is dominant, and therefore the parasinuous mode is stabilized at any value of E_u.

In the present model the electrical Euler number E_u represents the relative magnitude of the tangential electrostatic

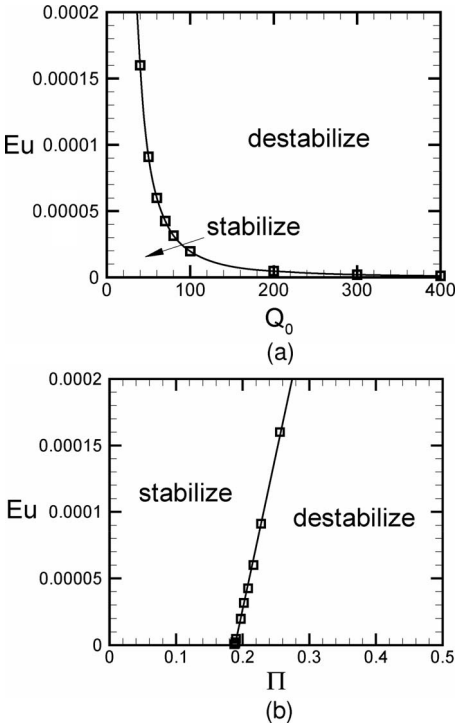

FIG. 5. (a) Boundary curve on the Q_0-E_u plane for the parasinuous mode, and (b) corresponding boundary curve on the Π-E_u plane. Q_0: the dimensionless surface charge density; E_u: the electrical Euler number; and $\Pi=Q_0^2E_u$: the combined dimensionless parameter.

force and the inertial force. On the other hand, the relative magnitude of the normal electrostatic force and the inertial force can be represented by a combined dimensionless parameter, i.e., $\Pi=q_0^2/\varepsilon_3\rho_2U_{2\text{out}}^2=Q_0^2E_u$. These two parameters are well representative of the axial and radial electric fields, respectively, in this theoretical model. We replotted the boundary curve in Fig. 5(a) on the Π-E_u plane in order to better understand the relation between the axial and radial electric fields in jet instability. Figure 5(b) illustrates the corresponding boundary curve on the Π-E_u plane. Obviously, the boundary curve between the stabilization and destabilization regions is nearly linear. Using the least-squares method, the curve is fitted as $E_u=0.002\,33\Pi-0.000\,438$ approximately. Note that the value of Π is much larger than that of E_u. That is, we need much stronger radial electric field to destabilize the parasinuous mode when axial electric field is imposed. Note also that the value of E_u itself is considerably small. It implies that the parasinuous mode is very sensitive to axial electric field. Considering that the present theoretical model is too complicated, we propose a simple model to evaluate the effect of the axial and radial electric fields on the jet instability in the following.

Consider a single-liquid jet with a charged inviscid liquid of infinite conductivity subjected to a uniform axial electric field. Suppose the basic velocity profile of the jet is uniform. When the jet is perturbed by an infinitesimal three-dimensional disturbance, a temporal linear instability analysis gives the dispersion relation in the dimensional form as follows [34,36]:

$$\rho(\omega+ikU)^2-\frac{\gamma k}{R^2}\frac{I_n'(kR)}{I_n(kR)}[1-n^2-(kR)^2]+\frac{q_0^2k}{\varepsilon_3R}\frac{I_n'(kR)}{I_n(kR)}\left(1+kR\frac{K_n'(kR)}{K_n(kR)}\right)+k^2E_0^2(\varepsilon-\varepsilon_3)-ik^2q_0E_0\frac{K_n'(kR)}{K_n(kR)}=0, \tag{37}$$

where ρ, U, γ, R, and ε are the density of liquid, the velocity of jet, the surface tension coefficient, the jet radius, and the electrical permittivity of liquid, respectively. ω and k are the dimensional complex eigenfrequency and axial wave number. The other parameters are the same with that in the present paper. There are five terms in the dispersion relation (37). They represent the effects of the inertia, surface tension, surface charge (i.e., radial electric field), axial electric field, and coupling of the surface charge and axial electric field, respectively. The balance of the third and fourth terms gives a simple ratio of the characteristic tangential electrostatic force and normal electrostatic force, i.e.,

$$\frac{\varepsilon_3^2E_0^2}{q_0^2}\sim\frac{1}{k(\varepsilon_r-1)}\frac{I_n'(k)}{I_n(k)}\left(1+k\frac{K_n'(k)}{K_n(k)}\right), \tag{38}$$

where k is the dimensionless wave number scaled by $1/R$, and $\varepsilon_r=\varepsilon/\varepsilon_3$. Apparently, the relative magnitude of the characteristic tangential and normal electrostatic forces is determined by the dimensionless wave number and the relative permittivity of liquid. Suppose $\varepsilon_r=80$, $k=1$. For the axisymmetric instability $n=0$, the ratio in Eq. (38) is -0.0024, where the negative sign indicates that the axial and radial electric fields have the opposite effect on jet instability. The calculation result shows that in the long wave region where the wave number k is of the order of unit, the ratio in Eq. (38) is always a small number, indicating that the characteristic tangential electrostatic force is much smaller than the characteristic normal electrostatic force. This explains why the dimensionless parameter E_u is small compared to the combined dimensionless parameter Π as found in Fig. 5(b). On the other hand, the balance of the first term with the fourth term in Eq. (37) gives the ratio of the tangential electrostatic force to inertial force, i.e.,

$$\frac{\varepsilon_3E_0^2}{\rho U^2}\sim\frac{(\omega+ik)^2}{(\varepsilon_r-1)}, \tag{39}$$

where ω and k are the dimensionless eigenfrequency and wave number scaled by U/R and $1/R$, respectively. For typical values $\varepsilon_r=80$, $k=1$, and $\omega_r=0.01$, the above ratio is 1.25×10^{-6} approximately. Apparently, the characteristic tangential electrostatic force is considerably small compared with the inertial force. This explains why E_u is so small in Figs. 4 and 5.

For the helical mode, the neutral stability curve on the Q_0-E_u plane and Π-E_u plane are plotted in Figs. 6(a) and 6(b), respectively. In the region marked with "unstable," the helical mode is unstable under the influence of the axial and radial electric fields. However, in the region marked with "stable," the mode is stable. As shown in Fig. 6(a), as surface

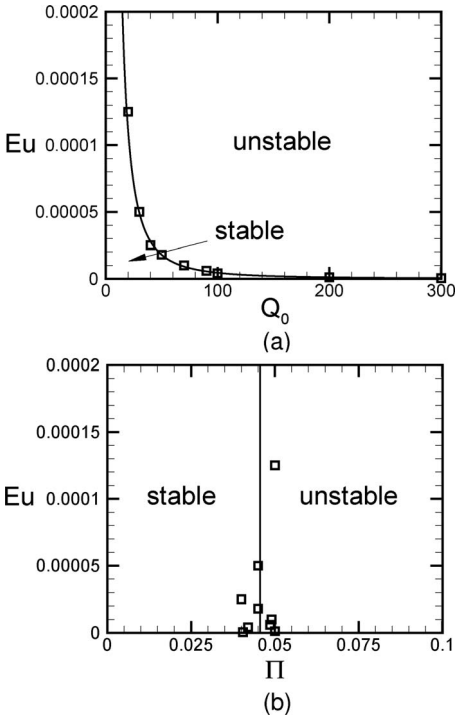

FIG. 6. (a) Neutral stability curve on the Q_0-E_u plane for the helical mode, and (b) corresponding neutral stability curve on the Π-E_u plane. Q_0: the dimensionless surface charge density; E_u: the electrical Euler number; and $\Pi = Q_0^2 E_u$: the combined dimensionless parameter.

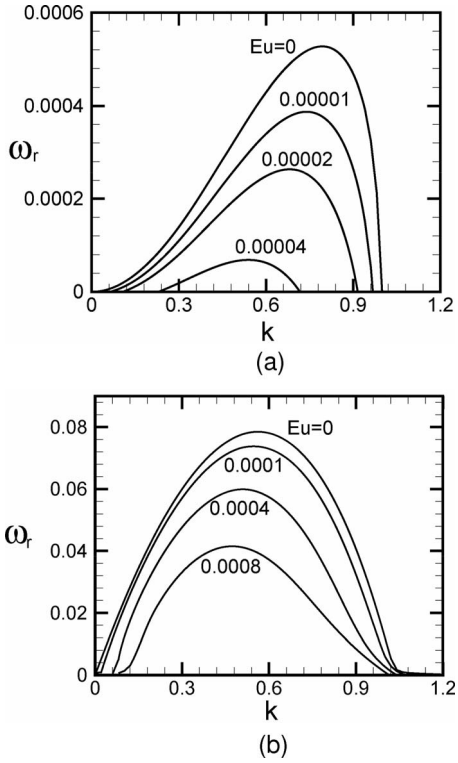

FIG. 7. Influence of the electrical Euler number E_u on the growth rate ω_r of (a) the paravaricose mode and (b) the parasinuous mode at zero surface charge density and low liquid viscosity. $\mu_r = 1$.

charge density increases, the mode is easier to destabilize. However, when surface charge density is sufficiently small, the mode is stable no matter how large E_u is. On the Π-E_u plane the neutral stability curve is approximately a vertical straight line with $\Pi = 0.0456$, regardless of the value of E_u. (The spreading of data at random may be caused by calculation error.) As the electric field increases, the helical instability first occurs in the long wave region where $k \to 0$, and in this limit the fourth term is infinitely small compared with the third term in the dispersion relation (37). Therefore the neutral stability curve is not affected by the axial electric field. Note that E_u is much smaller than Π. Here we also use the simple single-liquid jet model to estimate the relative magnitude of the characteristic normal and tangential electrostatics forces. Let $n = 1$, Eq. (38) results in

$$\frac{\varepsilon_3^2 E_0^2}{q_0^2} \sim \frac{1}{k(\varepsilon_r - 1)} \frac{K_0(k)}{K_1(k)} \left(1 - k \frac{I_0(k)}{I_1(k)}\right). \tag{40}$$

For typical values $\varepsilon_r = 80$, $k = 1$, we have $\varepsilon_3^2 E_0^2 / q_0^2 \approx -0.0110$. Apparently, the tangential electrostatic force is a small quantity relative to the normal electrostatic force, as shown in Fig. 6(b). Moreover, it can be testified that the characteristic tangential electrostatic force is much smaller than the inertial force. It indicates that the electrical Euler number E_u is a small number. Although the growth rate of the helical mode is greatly affected by the axial electric field, the neutral stability curve seems to be insensitive to the axial electric field. In addition, the calculation result shows that the helical mode, instead of the parasinuous mode, dominates the jet instability quickly as long as it becomes unstable. Therefore the neutral curve in Fig. 6 can also be regarded as the boundary curve between the helical instability dominant region and axisymmetric instability dominant region.

B. Case of small liquid viscosity

In the above section, it is found that the boundary curve between the axisymmetric and helical dominant regions is close to the neutral stability curve of the helical mode. We owe this phenomenon to the high viscosity of the inner liquid. In the reference state, the inner liquid is supposed to be sunflower oil with high viscosity, so the viscosity ratio of the inner and outer liquids $\mu_r = 43$. In this section a small viscosity case is considered (suppose $\mu_r = 1$). In this small viscosity case, we calculate the growth rate of the unstable modes at low and high surface charge densities, respectively.

Figures 7(a) and 7(b) illustrate the growth rates of the paravaricose mode and parasinuous mode, respectively, where the dimensionless surface charge density $Q_0 = 0$. Compared with Fig. 3, in such a low viscosity case the modes have much larger growth rate, indicating that the viscosity has a stabilizing effect on jet instability. The stabilization effect of viscosity is obviously due to energy dissipation caused by it. The parasinuous mode is still dominant. The helical mode is stable owing to the absence of surface charge. Figures 8(a) and 8(b) illustrate the growth rates of the parasinuous mode and helical mode, respectively, at a

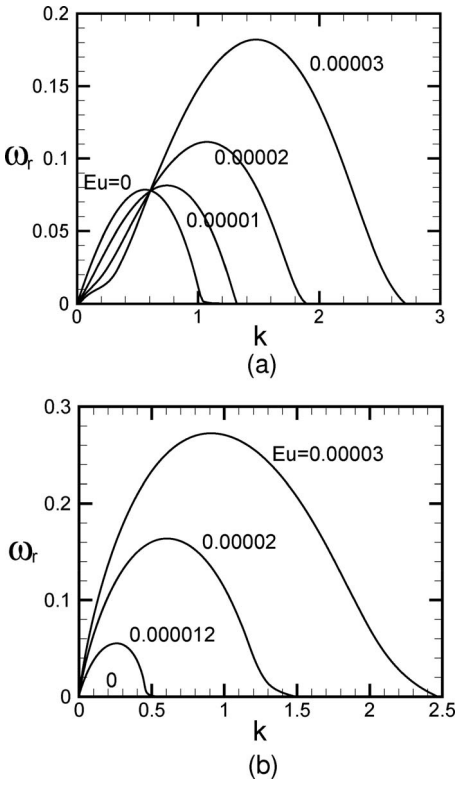

FIG. 8. Influence of the electrical Euler number E_u on the growth rate ω_r of (a) the parasinuous mode and (b) the helical mode at high surface charge density and low liquid viscosity. $Q_0=100$ and $\mu_r=1$.

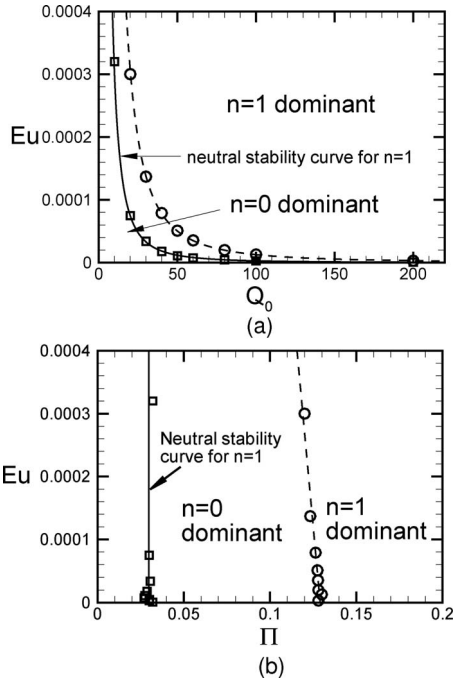

FIG. 9. (a) Neutral stability curve for the helical mode (solid) and boundary curve between the axisymmetric instability ($n=0$) and helical instability ($n=1$) dominant regions (dashed) on the Q_0-E_u plane, and (b) corresponding curves on the Π-E_u plane. $\mu_r=1$. Q_0: the dimensionless surface charge density; E_u: the electrical Euler number; and $\Pi=Q_0^2E_u$: the combined dimensionless parameter.

high surface charge density $Q_0=100$. Compared with Fig. 4, both the parasinuous mode and helical mode become more unstable, particularly the parasinuous one. Accordingly, the viscosity depresses the helical instability as well as the axisymmetric instability [37]. Comparing the growth rates of these two modes as shown in Fig. 8, it is clear that they are close. That is, in such a low viscosity case, the helical mode is dominant no more.

In the small viscosity case the neutral stability curve of the helical mode on the Q_0-E_u plane and Π-E_u plane are plotted in Figs. 9(a) and 9(b), respectively (solid curves). Compared with Fig. 6(a) the neutral stability curve moves toward the left and down on the Q_0-E_u plane. The unstable region of the helical mode is enlarged. On the Π-E_u plane the neutral stability curve of the helical mode is still a vertical straight line as shown in Fig. 6(b), but the value of Π is 0.0298, which is smaller than that in the case of high viscosity. Accordingly in the relatively low viscosity case the helical mode is easier to be destabilized by surface charge.

In addition, the boundary curve between the axisymmetric and helical dominant regions on the Q_0-E_u plane and Π-E_u plane are plotted in Figs. 9(a) and 9(b), respectively (dashed curves). Compared with Fig. 6(a) it is clear that the boundary curve moves toward the right upper corner. The helical dominant region is shrunk. That is, in the small viscosity case the helical mode requires a larger axial electric field and surface charge to become dominant. On the Π-E_u plane shown in Fig. 9(b), the boundary curve between the axisymmetric and helical instability dominant regions is linear, which is fitted as $E_u=0.003\,84-0.0298\Pi$ approximately. Comparing the boundary curves in Figs. 6 and 9, it is concluded that higher viscosity favors the predominance of the helical mode and helps the realization of coaxial electrospinning in experiments. In single-liquid electrospinning experiments [40,41], it was found that higher liquid viscosity and higher surface charge density helps the helical instability dominate in the process of jet breakup. Our result accords well with the experimental results; but why high viscosity dampens the axisymmetric instability more than the helical instability remains unknown. The physical mechanism with quantitative estimates needs to be uncovered in the future.

IV. CONCLUSION

A theoretical model of a charged viscous coaxial jet in an axial electric field is developed in the present paper. The outer liquid is considered as a leaky dielectric and the inner liquid a perfect dielectric. The eigenvalue problem is formulated and solved numerically. The temporal linear instability analysis is performed. The competition between the axisymmetric instability and helical instability is studied.

It is found that for the helical instability there exists one unstable mode in the long wavelength region, called the helical mode. The axial electric field and surface charge have great effects on the helical mode as well as on the axisymmetric modes, the former stabilizing the modes and the latter

destabilizing the modes. When the surface charge density is sufficiently small, the helical mode is stable and the parasinuous mode is dominant in jet instability. However, when the surface charge density is sufficiently large, the helical mode becomes unstable and dominates in jet instability as the electric field is enhanced. Liquid viscosity is found to have a vital effect on the predominance of the helical mode. Although at relatively small viscosity the helical mode becomes unstable easily, at relatively large viscosity it is easier to observe the helical instability in experiments.

ACKNOWLEDGMENTS

The authors are indebted to the reviewer for valuable comments that helped to improve the paper. The work was supported by the National Natural Science Foundation of China Project No. 10572137.

APPENDIX A: ELECTRIC FIELD PERTURBATIONS

It is obvious that the characteristic function of the electrical potential perturbation, $\hat{\psi}_m(r)$, satisfies the modified Bessel equation of order n,

$$\frac{d^2\hat{\psi}_m}{dr^2} + \frac{1}{r}\frac{d\hat{\psi}_m}{dr} - \left(k^2 + \frac{n}{r^2}\right)\hat{\psi}_m = 0, \quad n = 0,1.$$

The solutions are

$$\hat{\psi}_1 = A_1 I_n(kr),$$

$$\hat{\psi}_2 = A_2 I_n(kr) + A_3 K_n(kr),$$

$$\hat{\psi}_3 = A_4 K_n(kr),$$

where $I_n(kr)$, $K_n(kr)$ are the nth-order modified Bessel functions of the first and second kinds, respectively, A_1–A_4 are coefficients to be determined by boundary conditions. Substituting them into the boundary conditions (17)–(20) and keeping the linear terms, we obtain

$$A_4 K_n(k) = A_2 I_n(k) + A_3 K_n(k) + Q_0\hat{\eta}_2, \tag{A1}$$

$$A_1 I_n(ka) = A_2 I_n(ka) + A_3 K_n(ka), \tag{A2}$$

$$\varepsilon_{r1} A_1 I_n'(ka) = \varepsilon_{r2}[A_2 I_n'(ka) + A_3 K_n'(ka)] - i\hat{\eta}_1(\varepsilon_{r1} - \varepsilon_{r2}), \tag{A3}$$

$$\hat{q}_s = -\hat{\eta}_2[Q_0 + ik(1-\varepsilon_{r2})] - kA_4 K_n'(k) + k\varepsilon_{r2}[A_2 I_n'(k) + A_3 K_n'(k)], \tag{A4}$$

$$(\omega + ik)\hat{q}_s - Q_0\frac{d\hat{u}_{2r}}{dr} + ikQ_0\hat{\eta}_2\frac{dU_{2z}}{dr} + k\tau\varepsilon_{r2}[A_2 I_n'(k) + A_3 K_n'(k) + i\hat{\eta}_2] = 0, \tag{A5}$$

where the prime denotes the derivative of the corresponding Bessel functions with respect to the argument. The coefficients A_1–A_4 are expressed as the functions of $\hat{\eta}_1$, $\hat{\eta}_2$, and $\hat{q}_s$ by solving Eqs. (A1)–(A4). Then substituting them into the dynamic boundary conditions (11)–(14) and the surface charge conservation equation (A5), we obtain Eqs. (31) and (33)–(36).

APPENDIX B: EXPRESSIONS OF THE SYMBOLS

$$\Delta_0 = I_n(ka)K_n(k) - K_n(ka)I_n(k), \quad \Delta_1 = -I_n(ka)K_n'(k) + K_n(ka)I_n'(k),$$

$$D_1 = -K_n'(k)\left(1 - \frac{\varepsilon_{r2}}{\varepsilon_{r1}}\right) + I_n'(k)\left(\frac{K_n(ka)}{I_n(ka)} - \frac{\varepsilon_{r2}}{\varepsilon_{r1}}\frac{K_n'(ka)}{I_n'(ka)}\right),$$

$$D_2 = K_n(k)\left(1 - \frac{\varepsilon_{r2}}{\varepsilon_{r1}}\right) - I_n(k)\left(\frac{K_n(ka)}{I_n(ka)} - \frac{\varepsilon_{r2}}{\varepsilon_{r1}}\frac{K_n'(ka)}{I_n'(ka)}\right),$$

$$D_3 = -\frac{1}{k}\frac{D_2}{D_2\frac{K_n'(k)}{K_n(k)} + D_1\varepsilon_{r2}}, \quad D_4 = -\frac{1}{k}\frac{\frac{i\varepsilon_{r2}(\varepsilon_{r1}-\varepsilon_{r2})}{\varepsilon_{r1}I_n'(ka)}}{D_2\frac{K_n'(k)}{K_n(k)} + D_1\varepsilon_{r2}},$$

$$D_5 = -\frac{1}{k}\frac{D_2\left[Q_0\left(1 + \frac{kK_n'(k)}{K_n(k)}\right) + ik(1-\varepsilon_{r2})\right]}{D_2\frac{K_n'(k)}{K_n(k)} + D_1\varepsilon_{r2}},$$

$$D_6 = \frac{1}{k}\frac{D_1}{D_2\frac{K_n'(k)}{K_n(k)} + D_1\varepsilon_{r2}},$$

$$D_7 = -\frac{1}{k}\frac{\frac{K_n'(k)}{K_n(k)}\frac{i(\varepsilon_{r1}-\varepsilon_{r2})}{\varepsilon_{r1}I_n'(ka)}}{D_2\frac{K_n'(k)}{K_n(k)} + D_1\varepsilon_{r2}},$$

$$D_8 = \frac{1}{k}\frac{D_1\left[Q_0\left(1 + \frac{kK_n'(k)}{K_n(k)}\right) + ik(1-\varepsilon_{r2})\right]}{D_2\frac{K_n'(k)}{K_n(k)} + D_1\varepsilon_{r2}}.$$

[1] L. Rayleigh, Proc. London Math. Soc. **10**, 4 (1882).
[2] J. Zeleny, Phys. Rev. **10**, 1 (1917).
[3] G. I. Taylor, Proc. R. Soc. London, Ser. A **280**, 383 (1964).
[4] G. I. Taylor, J. Fluid Mech. **22**, 1 (1965).
[5] G. I. Taylor, Proc. R. Soc. London, Ser. A **291**, 159 (1966).
[6] G. I. Taylor, Proc. R. Soc. London, Ser. A **313**, 453 (1969).
[7] J. R. Melcher, *Field-Coupled Surface Waves* (MIT, Cambridge, MA, 1963).
[8] D. A. Saville, Phys. Fluids **13**, 2987 (1970).
[9] D. A. Saville, J. Fluid Mech. **48**, 815 (1971).
[10] A. L. Huebner and H. N. Chu, J. Fluid Mech. **49**, 361 (1971).
[11] G. Artana, H. Romat, and G. Touchard, J. Electrost. **43**, 83 (1998).
[12] K. Baudry, H. Romat, and G. Artana, J. Electrost. **40**, 73 (1997).
[13] P. H. Son and K. Ohba, Int. J. Multiphase Flow **24**, 605 (1998).
[14] H. González, A. Ramos, and A. Castellanos, J. Electrost. **47**, 27 (1999).
[15] H. González, F. J. García, and A. Castellanos, Phys. Fluids **15**, 395 (2003).
[16] J. R. Melcher and G. I. Taylor, J. Fluid Mech. **1**, 111 (1969).
[17] D. A. Saville, Annu. Rev. Fluid Mech. **29**, 27 (1997).
[18] J. M. López-Herrera, P. Riesco-Chueca, and A. M. Gañán-Calvo, Phys. Fluids **17**, 034106 (2005).
[19] R. J. Turnbull, IEEE Trans. Ind. Appl. **28**, 1432 (1992).
[20] R. J. Turnbull, IEEE Trans. Ind. Appl. **32**, 837 (1996).
[21] A. J. Mestel, J. Fluid Mech. **274**, 93 (1994).
[22] A. J. Mestel, J. Fluid Mech. **312**, 311 (1996).
[23] E. R. Setiawan and S. D. Heister, J. Electrost. **42**, 243 (1997).
[24] A. F. F. Elhefnawy, B. M. H. Agoor, and A. E. K. Elcoot, Physica A **297**, 368 (2001).
[25] A. F. F. Elhefnawy, G. M. Moatimid, and A. E. K. Elcoot, ZAMP **55**, 63 (2004).
[26] A. E. K. Elcoot, Int. J. Non-Linear Mech. **41**, 1219 (2006).
[27] A. E. K. Elcoot, Physica A **375**, 411 (2007).
[28] A. E. K. Elcoot, Eur. J. Mech. B/Fluids **26**, 431 (2007).
[29] S. Korkut, D. A. Saville, and I. A. Aksay, Phys. Rev. Lett. **100**, 034503 (2008).
[30] G. Loscertales, A. Barrero, I. Guerrero, R. Cortijo, M. Márquez, and A. M. Gañán-Calvo, Science **95**, 1695 (2002).
[31] J. M. López-Herrera, A. Barrero, A. López, I. G. Loscertales, and M. Márquez, J. Aerosol Sci. **34**, 535 (2003).
[32] Z. C. Sun, E. Zussman, A. L. Yarin, J. H. Wendorff, and A. Greiner, Adv. Mater. (Weinheim, Ger.) **15**, 1929 (2003).
[33] J. H. Yu, S. V. Fridrikh, and G. C. Rutledge, Adv. Mater. (Weinheim, Ger.) **16**, 1562 (2004).
[34] F. Li, X. Y. Yin, and X. Z. Yin, Phys. Fluids **17**, 077104 (2005).
[35] F. Li, X. Y. Yin, and X. Z. Yin, Phys. Fluids **18**, 037101 (2006).
[36] F. Li, X. Y. Yin, and X. Z. Yin, Phys. Rev. E **74**, 036304 (2006).
[37] F. Li, X. Y. Yin, and X. Z. Yin, J. Fluid Mech. **596**, 285 (2008).
[38] J. Shen and X. Li, Acta Mech. **114**, 167 (1996).
[39] J. N. Chen and S. P. Lin, J. Fluid Mech. **450**, 235 (2002).
[40] H. Fong, I. Chun, and D. H. Reneker, Polymer **40**, 4585 (1999).
[41] W. Zuo, M. Zhu, W. Yang, H. Yu, Y. Chen, and Y. Zhang, Polym. Eng. Sci. **45**, 704 (2005).